Design and Real-Time Implementation of a Centralized Microgrid Control System With Rule-Based Dispatch and Seamless Transition Function

Chu Sun , Geza Joos , Syed Qaseem Ali , Jean Nicolas Paquin, Carlos Mauricio Rangel , Fares Al Jajeh , Ilja Novickij, and Francois Bouffard

Abstract—With reference to the newly released microgrid standards, design and real-time implementation of a centralized microgrid control system is presented in this article. In the grid-connected mode, the utility grid will provide the voltage and frequency reference at the point of connection. The assets within the microgrid will follow power command references provided by the control system. In the islanded mode, the energy storage system (ESS) can provide the voltage and frequency reference to all other generators. Based on the state-of-charge of the ESS, a rule-based dispatch is proposed, with priority given to diesel generator and then the storage in the middle state of charge range. To alleviate power fluctuations, meet smooth planned islanding requirement, and compensate for the feeder losses ignored in dispatch algorithm, a supplementary slack-bus power control based on closed-loop feedback and first-order filter is proposed. The potential of the storage system in firming short-time power fluctuation and providing long-term load shifting capabilities is exploited. An emergency dispatch function for unplanned islanding considering the speed of response limitation of a diesel generator is also proposed. The proposed control strategy is implemented and tested on a controller hardware-in-the-loop test bench. It demonstrates the capability of the control system to reduce load shedding and renewable curtailment, and to implement power management at the point of interconnection.

Index Terms—Controller hardware-in-the-loop (C-HIL) test, microgrid control system (MGCS), rule-based dispatch, slack-bus power control, smooth transition, state of charge (SoC) management.

I. INTRODUCTION

IN THE past decade, microgrids have drawn wide attention by researchers for their capability of providing resilient power supply and effective integration of distributed renewable resources (DERs). To facilitate wider acceptance and further deployment, the core function specifications for a microgrid control system (MGCS) or microgrid controller and the corresponding tests have been standardized [1]. In accordance to IEEE Std 2030.7, "dispatch" and "transition" are the two core functions of MGCS [2]. Dispatch function refers to the coordination of DERs in a microgrid to maintain power balance, while achieving objectives including power fluctuation alleviation, total cost minimization, carbon emission reduction, or supply reliability maximization. To enhance energy security and continuous operation, it is expected that microgrids should be transited seamlessly between the grid-connected mode and the islanded mode. Once a microgrid controller is designed, an associated set of test platform is required for validation and compliance testing of the controller. According to IEEE Std 2030.8, controller hardware-in-the-loop (C-HIL) test is superior to purely simulation test and power hardware-in-the-loop test for its balance in "fidelity" and "coverage" [3].

There are numerous real-time implementations of MGCS found in the literature. However, most of the existing microgrid control test-bench may only focus on one specific function, and the tests are conducted without conforming to an acknowledged standard. In [4], the state-space-node approach and field-programmable gate array (FPGA)-based computation engine are adopted for real-time simulation of microgrids, but neither dispatch nor transition function was tested. A C-HIL testbench implementing constant power at point of interconnection (POI) in the grid-connected mode and fixed-frequency control in the islanded mode is developed in [5], but transition and dispatch function are not fully tested. A universal C-HIL platform for microgrid controller testing is proposed in [6], but only transition function is tested. In [7], an MGCS embedded with dispatch function is validated on a real-time testbed, but the optimization is still run offline. Similarly, dispatch and protection functions are presented in [8], but no comprehensive tests are conducted.

On the other hand, most microgrids are not complex enough to warrant a dispatch function based on the optimization algorithm. In IEEE Std 2030.7, the term "dispatch rules" is repetitively mentioned possibly due to its simplicity and low cost in implementation while "optimization function" is labeled with "if applicable." However, the standard does not deliberate on the specific dispatch rule design. In [9], a control scheme with the energy storage system (ESS) used for power smoothing and state of charge (SoC) fixed around 0.5 is proposed for grid-connected and islanded operation modes. Though the SoC can be strictly controlled, it is quite conservative since the capability of ESS as energy buffer to fulfill peak shaving and valley filling is not explored at all. A comparative study of load-following control and cycle-charging control applied to an islanded PV-diesel-ESS microgrid is conducted in [10] where the ESS and diesel generator, respectively, are used as the main source to fulfill power balance. It is revealed that employing ESS to follow load variation can reduce fuel consumption but may soon exhaust the energy stored [11]. Conventional cycle-charging strategy with ESS frequently deep discharged will shorten the lifetime of ESS. Considering the above limitations, a hybrid adaptive rule-based dispatch with diesel generator and energy storage selected alternatively to meet power mismatch in different SoC ranges for a practical stand-alone microgrid is reported in [12]. However, the control strategy still cannot realize direct SoC management.

In response to microgrid controller standardization, a centralized MGCS is designed and implemented in this article, based on the authors' precedent work [11]. The rule-based dispatch strategy is improved so that load shedding and renewable curtailment are replaced by POI power adjustment in the grid-connected mode. SoC of ESS can also be explicitly managed by forced charging or discharging control if SoC is beyond some threshold. The tie-line control in [11] is now generalized as slack bus power control to mitigate the power fluctuation at POI and compensate for the ignored feeder losses. Seamless transition control in the islanding and reconnection process is also presented. The control strategy is implemented with a C-HIL test-bench, with multiple test scenarios presented to demonstrate its effectiveness.

II. MICROGRID CONTROL STRATEGY

A. Microgrid Configuration

According to the example microgrid topology in the standards, a simple microgrid with sufficient representation of asset diversity is adopted [2], which is composed of one directly connected diesel generator, one ESS, two renewable energy resources (RERs) including a type-4 wind-turbine generator (WTG) and a photovoltaic (PV) generator, one continuously curtailable load, and one critical load, as shown in Fig. 1. The system is connected to the utility grid with a breaker at POI.

B. Local Control Strategy

The voltage and frequency references are established by the utility grid in the grid-connected mode and by *Vf* controlled ESS in the islanded mode [13], [14]. The diesel generator
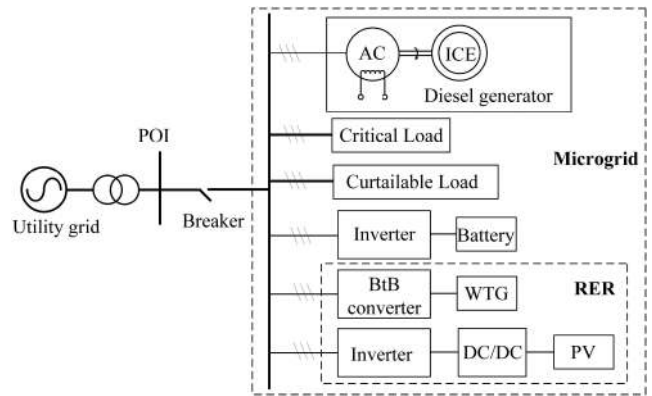

Fig. 1. Diagram of the microgrid under test.

TABLE I
CONSTRAINTS OF ASSETS IN THE MICROGRID

Parameters	Constraints
SoC and power of ESS	$SoC_{min} \leqslant SoC \leqslant SoC_{max}$ $P_{dis,max} \leqslant P_{ess} \leqslant P_{ch,max}$
Diesel generator power P_{diesel}	$P_{ds,min} \leqslant P_{diesel} \leqslant P_{ds,max}$

employs droop control with power reference determined by the dispatch strategy. RER-based generators (PV and WTG) adopt a maximum-power-point-tracking control by default.

C. Rule-Based Dispatch Strategy

On top of the local control level, a rule-based dispatch is designed as per the objectives in IEEE Std 2030.7 and 2030.8 [2], [3]. Basic constraints of the two controllable assets are summarized in Table I [12], [15]. SoC of ESS should be within an acceptable range (SoC_{min} and SoC_{max}) to avoid overcharging or overdischarging. The charging/discharging power limits $P_{ch,max}$ (positive) and $P_{dis,max}$ (negative) are restricted by storage and charging facilities. The diesel generator is kept ON to increase system reliability and reduce the start/stop impact. Its power should be controlled between minimum ($P_{ds,min}$) and maximum ($P_{ds,max}$) limit for efficient and secure operation. Since renewable curtailment or load shedding are mostly the last resorts to power balance in the islanded mode, their constraints are not presented. This article is focused mainly on active power dispatch given the major initiative of deploying microgrid. The main objectives include increasing reliability and resilience, reducing load shedding and RER curtailment, and meeting POI orders.

The local control and specific DER model may affect the transient performance. For example, the load model includes resistive load, power electronic load, motor load, or generally ZIP load, among which the induction motor load may result in oscillation or even instability in certain islanded microgrid [16]. However, from the power balance perspective, the calculation of load-generation mismatch will be the same independent of the model selected. In the current work, a constant power load based on the dynamic load model in RT-Lab is adopted for critical load.
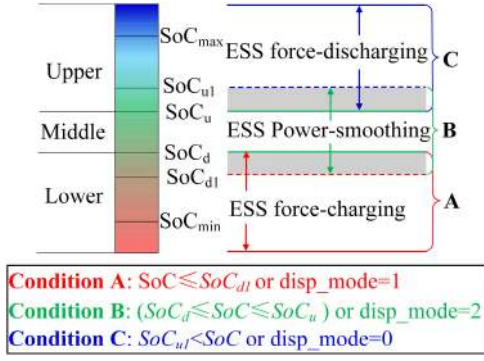
Fig. 2. Allocation of control modes in different SoC ranges.

The curtailable load adopts a general power-electronic interfaced load mode [17].

1) Dispatch in the Islanded Mode: To maintain power balance, the net power P_{net} is defined by (1) as the difference between the RER generation P_{rer} and total load consumption P_{load}

$$P_{net} = P_{rer} - P_{load} = P_{wtg} + P_{pv} - P_{load}. \quad (1)$$

According to [15], the reliability and resilience of microgrid is a quadratic function of SoC which should be preferably kept around 0.5 for bidirectional energy reserve. However, ESS can also fulfill energy shifting by storing energy and then releasing when necessary. Therefore, the practical SoC may slightly deviate from 0.5 to perform this function. To achieve both objectives, a rule-based dispatch in the form as decision trees is proposed, by dividing the SoC of ESS into three overlapped ranges [18] with four customizable SoC levels (SoC_{u1}, SoC_u, SoC_d, and SoC_{d1}), as shown in Fig. 2. The flowcharts of the rule-based dispatch are given in Fig. 3 where the curtailable load and RERs are not shed or curtailed by default. The power references for diesel generator, ESS, load shedding and renewable are denoted by $P_{ds,ref}$, $P_{ess,ref}$, P_{ld_shed}, and P_{rer_cur}, respectively.

In the lower SoC range (below SoC_{d1}), ESS force-charging control is adopted. ESS will get charged at a rate no smaller than $k_c * P_{ch,max}$ where k_c is an adjustable value within [0,1]. The power balance problem can be firstly formulated by the following inequalities (2) and solved by interval analysis [19]

$$\begin{cases} P_{ess,ref} - P_{ds,ref} = P_{net} \\ k_c * P_{ch,max} \leq P_{ess,ref} \leq P_{ch,max} \\ P_{ds,min} \leq P_{ds,ref} \leq P_{ds,max}. \end{cases} \quad (2)$$

Details of the dispatch are described by the numbered commands (c#1–4) in Fig. 3(a). If the value of P_{net} is within the subtracted interval of diesel generator power and ESS charging power, as calculated by (3), ESS will charge as

$$k_c * P_{ch,max} - P_{ds,max} \leq P_{ess,ref} - P_{ds,ref} \leq P_{ch,max} - P_{ds,min} \quad (3)$$

much as possible without exceeding $P_{ch,max}$, while diesel generator power will maintain power balance (c#1–2). Otherwise,
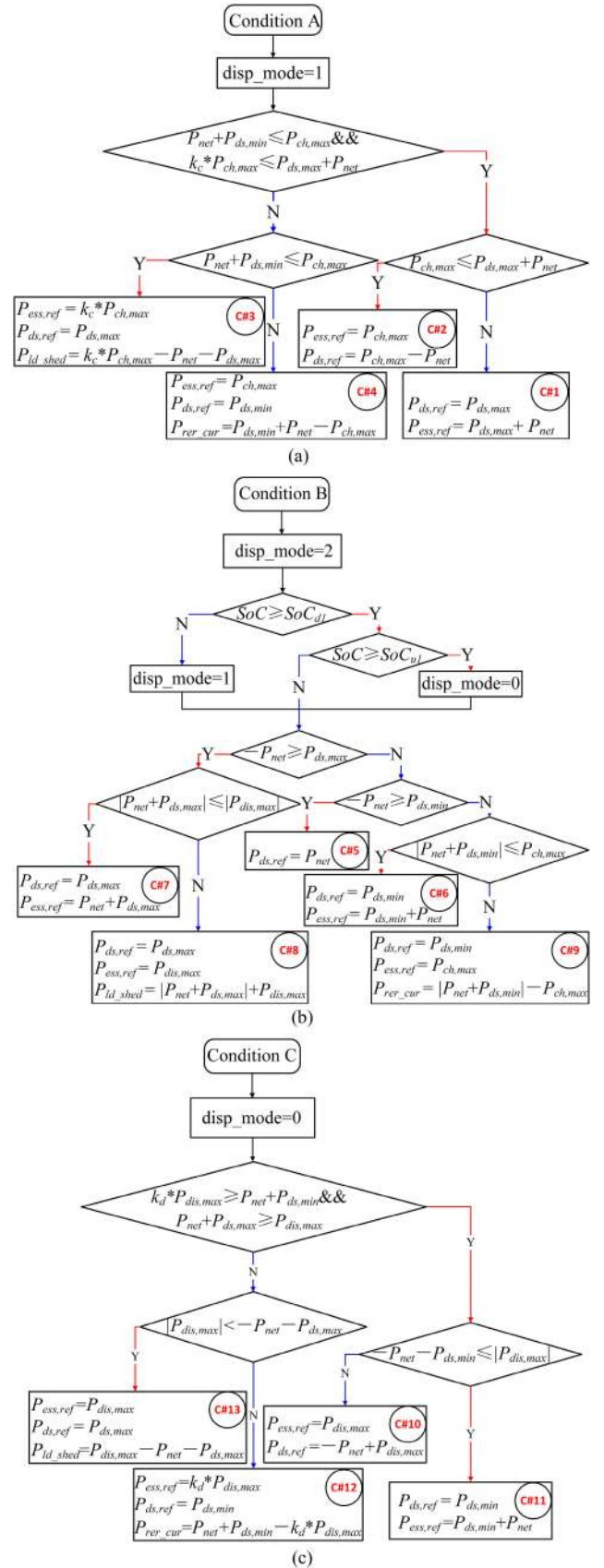

Fig. 3. Dispatch of DERs in microgrid. (a) ESS force-charging control. (b) ESS power-smoothing control. (c) ESS force-discharge control.

the problem (2) has no solution and load shedding or renewable curtailment must be adopted. If $P_{ds,\max}$ is insufficient, curtailable load will be shed (c#3); if ESS is to be charged more than $P_{\mathrm{ch},\max}$ even for $P_{ds,\min}$, renewable generation will be curtailed (c#4). The curtailed or shed amount is as small as possible as long as a solution exits.

Fig. 3(b) illustrates ESS power-smoothing control in the middle SoC range ([SoC_{d1}, SoC_{u1}]), by which diesel generator will be the main source to meet power mismatch, while the averaged power of ESS will be normally zero and its SoC will remain almost constant (c#5). However, if diesel generator alone cannot maintain power balance, ESS charging (c#6) or discharging (c#7), and load shedding (c#8), or renewable curtailment (c#9) will also be adopted.

In the upper SoC range (above SoC_{u1}), the system adopts ESS force-discharging control by which ESS is forced to discharge at a rate no smaller than $k_d * P_{\mathrm{dis},\max}$ where k_d is also adjustable, as shown in Fig. 3(c). As a duality to the problem (2), interval analysis can be utilized to generate the dispatch command. If P_{net} is within the subtracted interval of diesel generator power and ESS discharging power, ESS will discharge as much as possible while diesel generation will balance the remaining power(c#10–11). Otherwise, renewable curtailment (c#12) or load shedding (c#13) will force ESS to discharge without exceeding $P_{\mathrm{dis},\max}$.

To avoid possible consistent mode transitions on the boundaries of the three SoC ranges, a latching mechanism is established by introducing an auxiliary variable **disp_mode** which is "2" in power smoothing control, "1" in force-charge control and "0" in force-discharge control. The control mode will be determined by the conditions "A", "B," and "C" in Fig. 2. As further illustrated by the arrows and shaded region, the latching mechanism is realized by "or" logic and freezing the value of **disp_mode**. For example, in condition A, the MGCS will keep in force-charging mode until SoC reaches SoC_d. Given the three control modes, the relation of SoC and power of ESS can be calculated by (4) where C_{ess} is its energy capacity. Therefore, for whatever initial value of SoC at t_0, SoC of ESS will converge to the middle range

$$\mathrm{SoC}(t) = \mathrm{SoC}(t_0) + \int_{t_0}^{t} P_{\mathrm{ess}} dt / C_{\mathrm{ess}}$$

$$\begin{cases} P_{\mathrm{ess}} \geq k_c * P_{\mathrm{ch},\max}, \mathrm{SoC}(t_0) \leq \mathrm{SoC}_d \\ P_{\mathrm{ess}} \approx 0, \mathrm{SoC}_d \leq \mathrm{SoC}(t_0) \leq \mathrm{SoC}_u \\ P_{\mathrm{ess}} \leq k_d * P_{\mathrm{dis},\max}, \mathrm{SoC}(t_0) \geq \mathrm{SoC}_u. \end{cases} \quad (4)$$

Although the power references of ESS and diesel generator are explicitly given, no reference is needed if one of them serves as the slack bus. The renewable curtailment command will be distributed among WTG and PV based on certain criteria, for example in proportional to their output power before curtailment. The force-charging or discharging rate (k_c and k_d) is user-definable based on operator objectives or load/generation conditions. In this article, both are 0.05, representing a slow SoC recovery to avoid excessive load shedding or renewable curtailment to charge/discharge ESS.
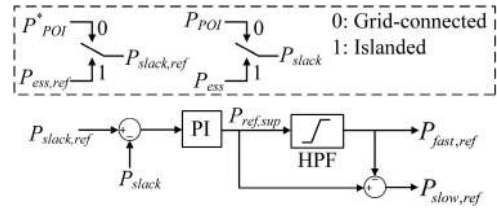

Fig. 4. Supplementary closed-loop control for slack bus power regulation.

Notice that this article only provides an example of rule-based dispatch strategies with the given constraints and objectives. If more constraints or other objectives are considered, the dispatch rules can be extended to those applications with proper modifications.

2) Dispatch in the Grid-Connected Mode: Reducing power variation at the POI is an extra objective in the grid-connected mode [2]. To meet the requirement of a specified power value P_{POI}^* at POI, the dispatch rules in Fig. 3 can still be used, with net power modified as (5), but P_{POI}^* will be adjusted instead of shedding load or curtailing renewable generators in Fig. 3

$$P_{\mathrm{net}} = P_{\mathrm{rer}} + P_{\mathrm{POI}}^* - P_{\mathrm{load}}. \quad (5)$$

3) Supplementary Slack-Bus Power Control: The dispatch rule in Fig. 3 is an open-loop control that ignores power fluctuation during the dispatch interval (5–15 min) and power losses in the feeders. The resulted error will be by default compensated by the slack bus, namely utility grid in the grid-connected mode and ESS in the islanded mode, which may violate the POI power request or the power and SoC constraints of ESS. For such, on the basis of tie-line power control in [11], [20], supplementary closed-loop feedback control for the slack bus is adopted, as depicted in Fig. 4. The power of slack bus P_{slack} is measured and compared with its reference $P_{\mathrm{slack, ref}}$. The error is then processed by a proportional integral (PI) controller and a supplementary power reference $P_{\mathrm{ref,sup}}$ is generated. Further passing through a high-pass filter, the fast-varying component $P_{\mathrm{fast,ref}}$ is assigned to ESS in the grid-connected mode (in the islanded mode, ESS will automatically undertake this part), whereas the slow-varying part $P_{\mathrm{slow,ref}}$ is added to the power reference of curtailable load, diesel generator or renewable generators in condition A, B, and C, respectively. The slack-bus power control will be especially meaningful in a planned-islanding process where POI power should be ideally controlled at zero.

D. Control Strategy for Transition Function

Planned islanding is composed of the following three steps:
1) Adjust generation to meet power constraint of the breaker (ideally zero) by setting $P_{\mathrm{POI}}^* = 0$;
2) Open the breaker when power through POI is below a threshold for a specified duration;
3) Switch control strategy of ESS from *PQ* control to *Vf* control.

For reconnection, synchronization criterion must be met before closing the breaker at POI, which is monitored by a synchrocheck relay (simulated in this article). The difference
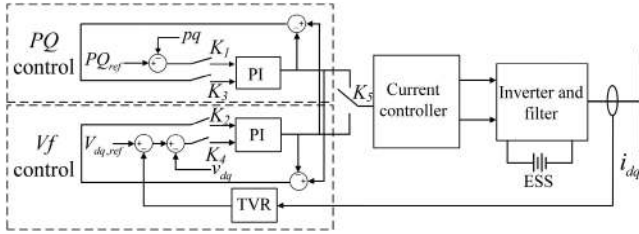
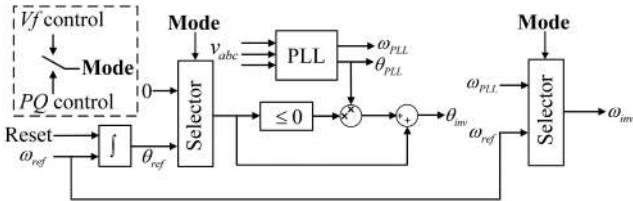Fig. 5.   *Vf* and *PQ* control for ESS with seamless transition features.

Fig. 6.   Phase angle saving and selection during transition.

Fig. 7.   Emergency dispatch rules for unplanned islanding.

Fig. 8.   Schematic diagram of the real-time MGCS testbench.

between frequency, phase angle, and voltage amplitude on both sides of the breaker, which can be measured by phase-locked loop (PLL), should be within a specified range [9], [21]–[22]. This can be achieved by active-synchronization, which sets voltage and frequency reference of ESS close to the values on the grid side of the breaker. After reconnection, ESS will be switched back to the *PQ* control mode.

To realize seamless transition, state-saving techniques are employed so that the current reference and phase angle generated within ESS are kept almost constant during transients [23], [24]. As illustrated in Fig. 5, for POI power control in the grid-connected mode, the switches K_1–K_2 are closed whereas K_3–K_4 are open. The switch K_5 is connected to *PQ* control output. Therefore, the output of *PQ* control is saved as the initial current reference for *Vf* control. In the islanded mode, the state of switches will turn opposite. Similarly, the phase angle is also saved before in the transition process, as shown in Fig. 6. To further improve the dynamic performance, a transient virtual resistor control is adopted [11].

Emergency dispatch will be adopted when an unplanned islanding event happens and ESS will switch to *Vf* control thereafter. In Fig. 7, there are four commands based on P_{POI} and P_{diesel} before islanding [labeled with (i–1)]. Given the limited response speed of diesel generator, its power will be frozen after islanding detection. Power mismatch due to P_{POI} variation will be first met by ESS, and then by shedding load or curtailing renewables. The advantage of keeping diesel generator ON is also exhibited here as it can provide grid support to help power converter such as ESS ride through abnormal voltage and frequency, which may deviate significantly due to the loss of utility grid in power-electronic converter based microgrid [24]. For such microgrids, it may be favorable that power-electronic converters can emulate the behavior of synchronous generator or provide a grid-supporting function such as voltage or frequency sensitive droop control during the unplanned islanding process [25], [26].
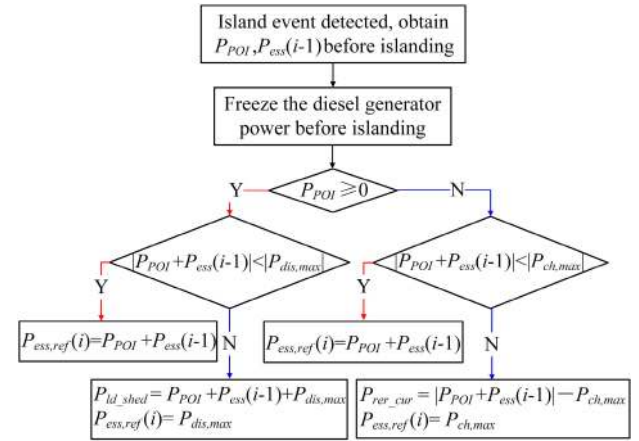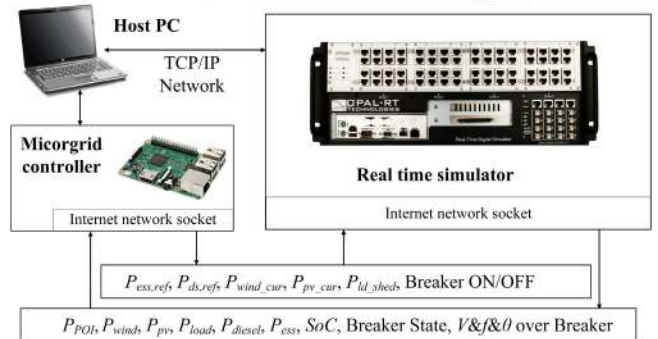
E. Reactive Power Dispatch

Assuming the considered microgrid is at low voltage level, reactive load is balanced by diesel generator and inverter-interfaced assets, while no SVC and FACTS devices are used. Reactive power is dispatched by weighting based on the remaining capacity defined as (6), where S_i is the power capacity, k_i is the steady-state overloading capability coefficient, and $P_{\text{ref},i}$ is active power reference of the i_{th} asset.

$$S_{\text{rem},i} = \sqrt{(k_i S_i)^2 - P_{\text{ref},i}^2}. \tag{6}$$

III. C-HIL IMPLEMENTATION OF MGCS

As shown in Fig. 8, the MGCS is implemented on a hardware controller Raspberry Pi. The microgrid model is running in OPAL-RT simulator OP5600, with an average power converter model employed to increase computational speed. The time step of real-time simulation is 50 μs. The required signals of the microgrid are transmitted to the centralized MGCS and control commands are sent back to the modeled assets. Internet communication based on UDP/IP protocol is used to interface MGCS with a real-time simulator. The control strategy is validated on a 600 V, 60 Hz three-phase ac microgrid. Parameters of the assets are listed in Table II, with base power being the maximum power capacity of DERs (320 kVA). The overloading capability of the

TABLE II
PARAMETERS OF THE MICROGRID ASSETS

Parameters	Value	Parameters	Values
Critical load	70 kW	WTG power capacity	200 kVA
Minimum curtailable load	20 kW	Diesel generator power capacity	320 kVA
ESS energy capacity	480 kWh	PV Power capacity	300 kVA
ESS power capacity	320 kVA	$P_{ds,min}$	96 kW
SoC_{max}	0.9	SoC_{min}	0.2
SoC_{ul}	0.75	SoC_u	0.6
SoC_d	0.5	SoC_{dl}	0.35

TABLE III
SCENARIOS FOR MGCS TESTS

Parameters	Scenarios		
	A	B	C
Initial SoC	25%	55%	90%
Average load power	1.8 p.u.	1.8 p.u.	1.5 p.u.
Average renewable power	0.3 p.u.	0.8 p.u.	1.6 p.u.

diesel generator is 1.5 p.u. whereas that of inverter interfaced DERs is 1.1 p.u.

IV. REAL-TIME TESTING OF MGCS

The general initial conditions for testing are specified in IEEE 2030.8 based on renewable energy output, load demand, and energy storage state-of-charge [3]. For brief testing the dispatch and transition function [27], Sections IV-A and IV-B presented three typical scenarios A–C listed in Table III, where ESS force-charging, power-smoothing, and force-discharging control will be adopted, respectively. In Section IV-C, a longer-time simulation with comparative tests will be conducted to validate the proposed dispatch strategy. The control interval may vary for different testing purposes.

A. Short-Term Test of Dispatch Function

For rapid verification, the renewable generation is purposely set to be highly fluctuant and the dispatch interval is selected to be 200 ms. The power of diesel generator, ESS, load, and renewable generator are denoted by P_{DS}, P_{ESS}, P_{load}, and P_{RER}, respectively.

1) Dispatch in the Grid-Connected Mode: In Fig. 9(a), the microgrid is under Scenario A and P_{POI}^* is 0.2 p.u. (import). Initially, diesel generator power is 0.5 p.u., whereas ESS has no output power. At $t = 40$ s, the dispatch rule (c#3) in Fig. 3(a) is enabled. Diesel generator increases its power to maximum $P_{ds,max}$ (1 p.u.) while P_{POI}^* is adjusted to be around 0.5 p.u. given the heavy loading situation. The feeder losses and power fluctuation will be reflected on P_{POI}, which can be compensated by slack-bus power control. ESS will provide the fast-varying component in the compensated power, while its average charging rate is around $k_c = 0.05$ p.u. The slow-varying component is undertaken by shedding load, as observed from the load decrease after $t = 40$ s.

In Fig. 9(b), the microgrid is under Scenario B. P_{net} is around 1 p.u., which will be first met by diesel generator and then
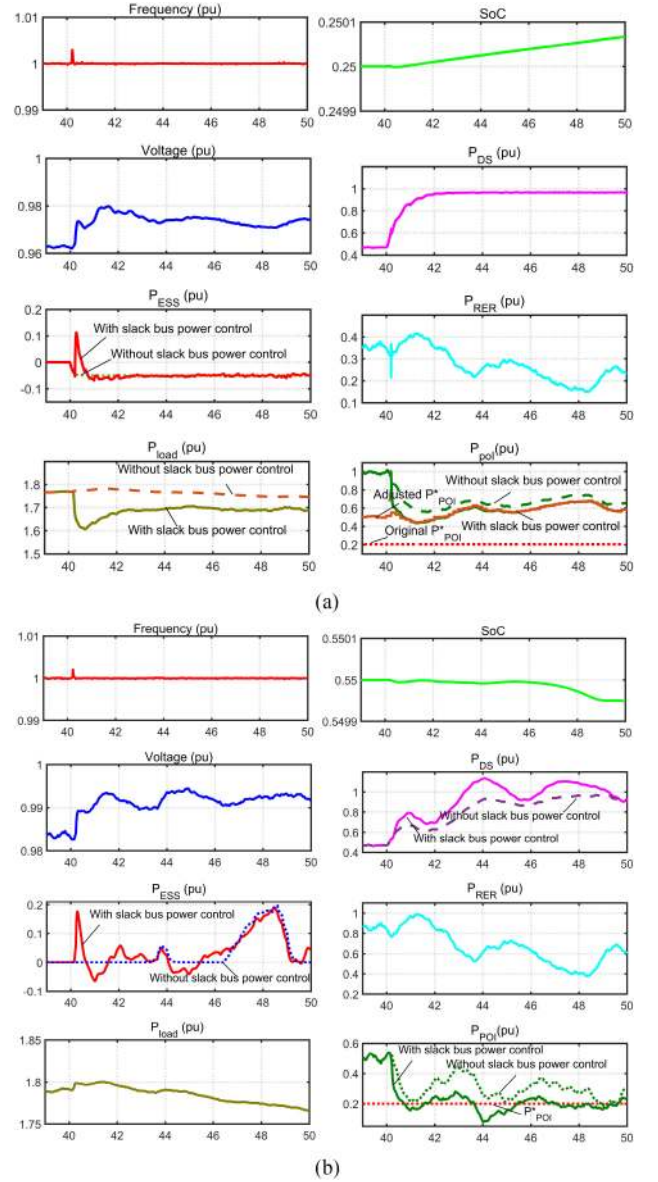

Fig. 9. Dispatch in the grid-connected mode with dispatch enabled at $t = 40$ s. (a) Under Scenario A. (b) Under Scenario B.

by ESS. The effect of the slack-bus power control can also be observed from the waveform of POI power. The slow-varying component will be supplied by diesel generator given its capability to provide more power.

2) Dispatch in the Islanded Mode: The ESS serves as the system reference in the islanded mode. In Fig. 10(a), microgrid is under Scenario A and ESS is forced to charge at power around 0.05 p.u. According to Command c#3 in Fig. 3(a), diesel generator outputs the maximum power $P_{ds,max}$ (1 p.u.) and curtailable load is shed. Due to the slack bus power control in Fig. 4, the feeder losses, for example 5%, which is originally compensated by *Vf* controlled ESS solely, will now be shared by both curtailable load and ESS. The ESS will only undertake the fast-varying component, without affecting the averaged charging power. Otherwise, ESS must countervail the feeder loss, and the original slow charging process will be further interfered.
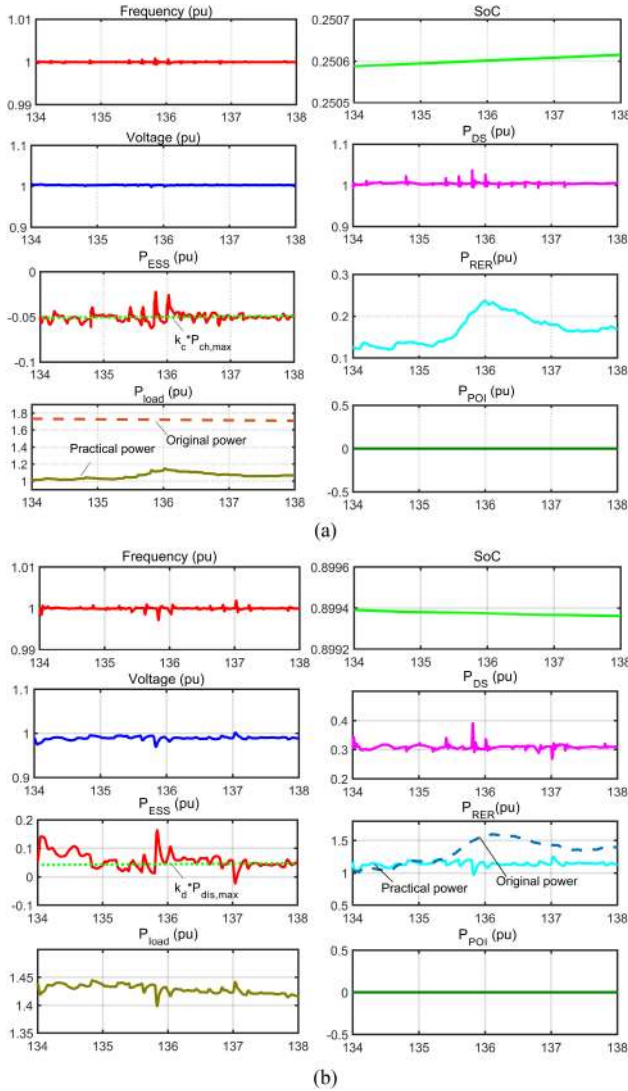
Fig. 10.   Dispatch in the islanded mode. (a) Under Scenario A. (b) Under Scenario C.

Fig. 11.   Results of planned islanding enabled at $t = 60$ s. (a) Under Scenario B. (b) Under Scenario C.

In Fig. 10(b), the microgrid is under Scenario C with excessive generation from RER. Diesel generation is reduced to the minimum limit $P_{ds,\min}$ (0.3 p.u.). By renewable curtailment and the slack bus power control, ESS is forced to discharge at the rate $k_d = 0.05$ p.u., which matches Command c#12 in Fig. 3(c).

B. Test of Transition Function

The test results of transition function are covered in this section, with a control interval at 20 ms.

1) Planned Islanding: In Fig. 11(a), a microgrid is under Scenario B and initially in the grid-connected mode. At $t = 60$ s, planned islanding command is released by changing P_{POI}^* from 0.2 p.u. to zero. With the slack bus power control, P_{POI} is controlled to be smaller than the threshold (0.05 p.u.) for 10 s. After that, microgrid gets islanded by opening the breaker at POI while ESS switches to *Vf* control. By observing the waveform, the islanding process is seamless because the state-saving techniques make the current reference and phase angle of ESS
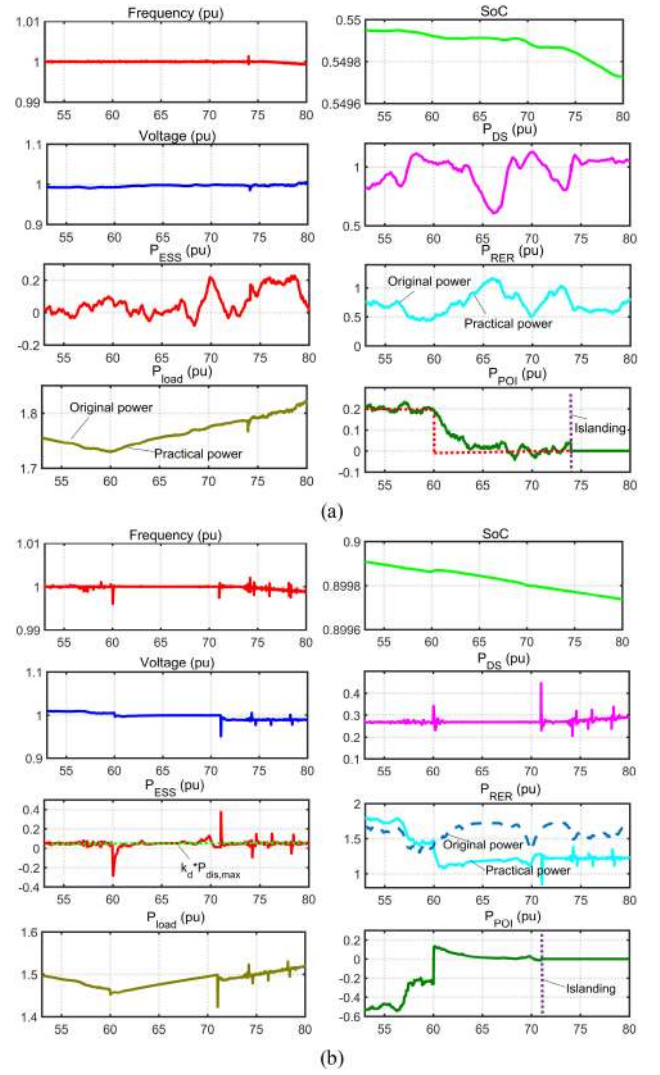
almost unchanged. Power of DERs has small changes due to the voltage variation after islanding.

The results of planned islanding under Scenario C is shown in Fig. 11(b). In this case, POI power adjustment will be disabled after $t = 60$ s and the POI power is controlled to be around zero by supplementary slack bus power control which will be fulfilled by ESS and renewable generator.

2) Reconnection: For resynchronization, the voltage, frequency, and phase angle on both sides of breaker are measured by PLL. Voltage reference of *Vf* controlled ESS is then set at the grid-side voltage (1 p.u. here), whereas its frequency reference is reduced from 60 to 59.9 Hz at a rate of 0.01 Hz/s. The phase angle difference over the breaker at POI will automatically change.

In Fig. 12(a), the microgrid is under Scenario B. At $t = 90.1$ s, synchronization criterion is met and the breaker at POI gets closed. ESS switches from *Vf* control to *PQ* control with active power reference identical to the output power before reconnection. Grid-connected dispatch rules and the slack bus power control is enabled thereafter, with P_{POI}^* being zero. The
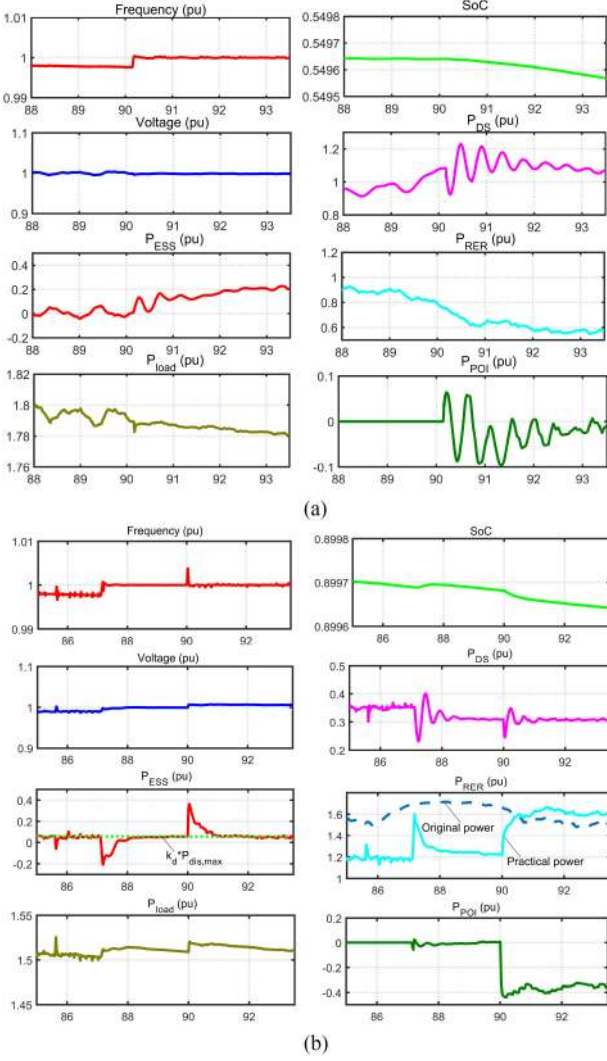
Fig. 12. Results of the reconnection process. (a) Under Scenario B. (b) Under Scenario C.
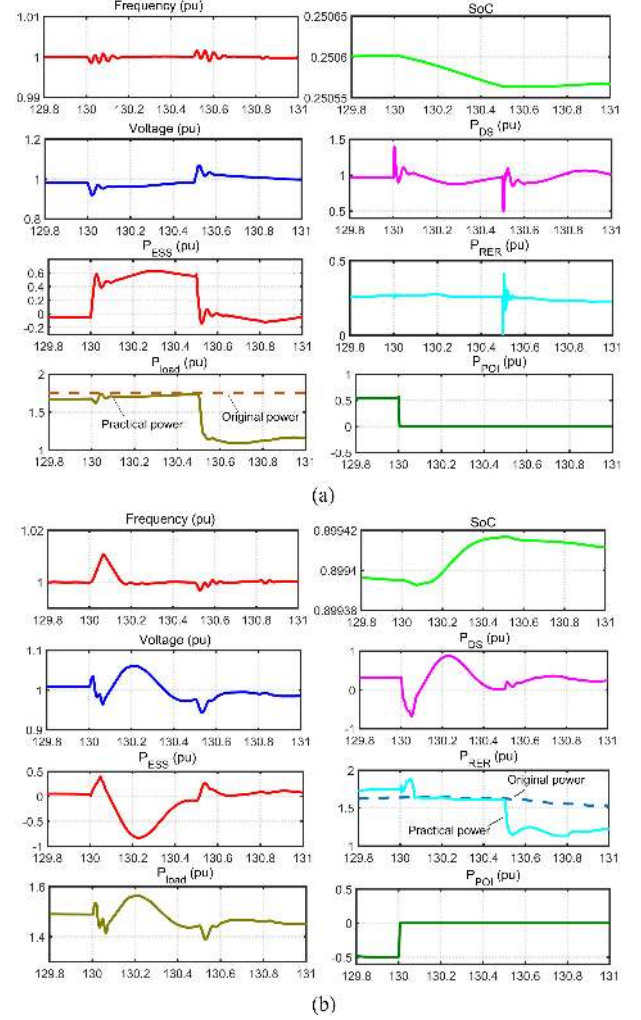

Fig. 13. Results of unplanned islanding. (a) Under Scenario A with ideal islanding detection. (b) Under Scenario C with 50 ms islanding detection delay.

reconnection process is almost seamless. The small power oscillation is due to the synchronization between diesel generator with the utility grid.

In Fig. 12(b), the microgrid is under Scenario C and reconnected at $t = 88.1$ s. Before reconnection, renewable is curtailed to force ESS discharge at 0.05 p.u. After $t = 90$ s, P_{POI}^* is readjusted to export, thus avoiding renewable curtailment. Due to frequency droop control, diesel generation is slightly larger than $P_{ds,min}$ before reconnection.

3) Unplanned Islanding: An unplanned islanding event occurs at $t = 130$ s. The breaker opens and P_{POI} drops to zero immediately.

In Fig. 13(a), the microgrid is under Scenario A and initially grid-connected. Diesel generator outputs maximum power $(P_{ds,max})$ and electricity is initially imported from the utility grid, forcing ESS to charge at 0.05 p.u. Assuming ideal islanding detection, emergency dispatch takes effect at $t = 130$ s. ESS picks up the power mismatch and switches to *Vf* control. Power outputs of other DERs remain almost unchanged in the emergency

dispatch till $t = 130.5$ s. After that, islanded dispatch rule is adopted. Power mismatch will then be met by load shedding instead of ESS discharging, and ESS will continue to be charged at 0.05 p.u.

In Fig. 13(b), the microgrid is under Scenario C and power is initially exported to the utility grid. By emergency dispatch, power mismatch due to P_{POI} change will be met by ESS. A delay of 50 ms is assumed between the islanding event and emergency dispatch action. The voltage and frequency deviation are therefore larger than in Fig. 13(a). However, because diesel generator is essentially a voltage source, the impact due to islanding detection delay will be smaller than the microgrid with purely *PQ* controlled power-electronic converters in unplanned islanding process [11].
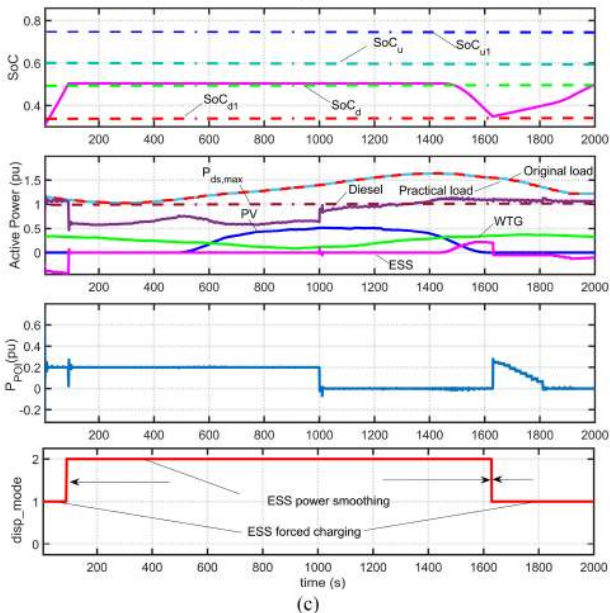
C. Daily-Scale Test of Dispatch Function

To quickly validate the dispatch function on a daily scale, the 24-h power profile is scaled to 2000 s and the original dispatch interval 10 min is scaled to 14 s.
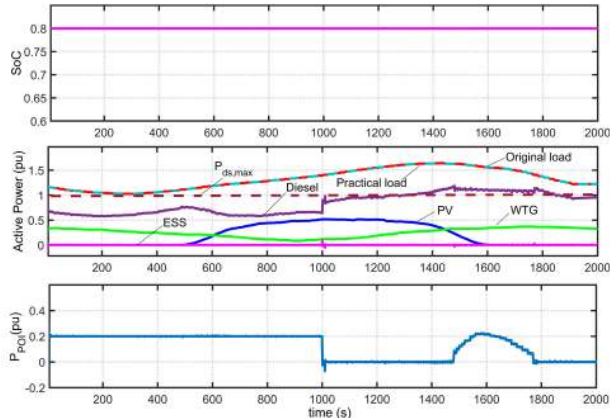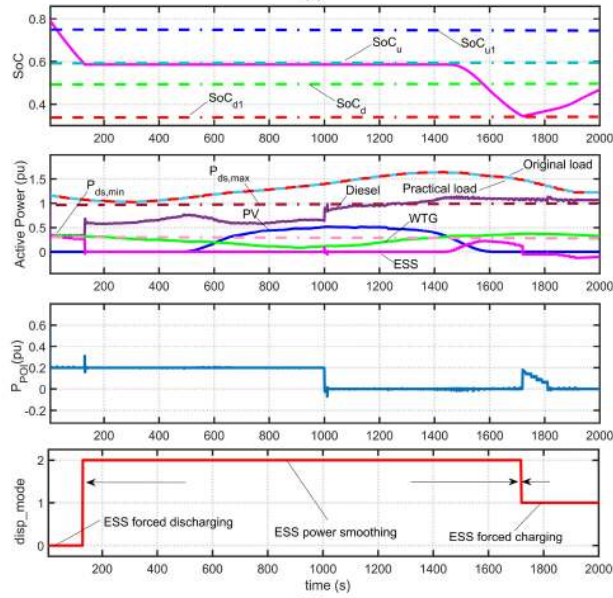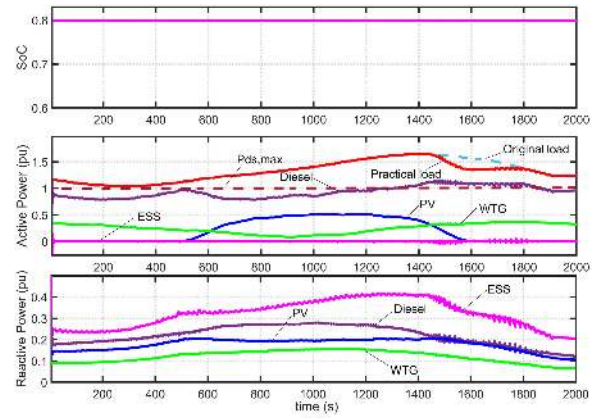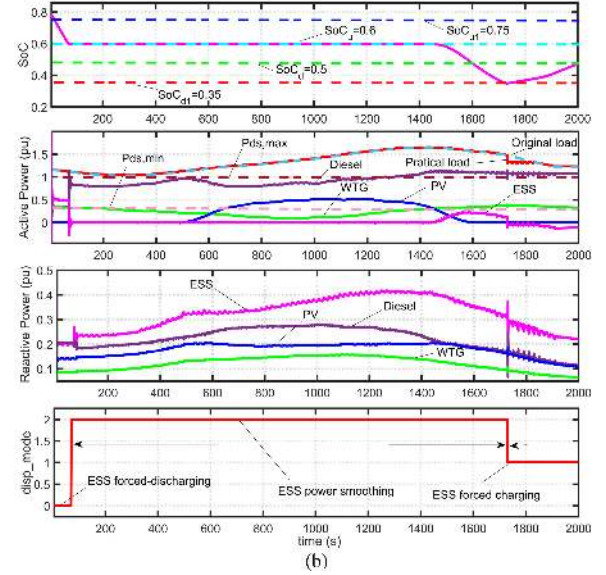
Fig. 14. Results of daily-scale dispatch in the grid-connected mode. (a) Conventional power smoothing control with initial SoC at 0.8. (b) Proposed control strategy with initial SoC at 0.8. (c) Proposed control strategy with initial SoC at 0.3.

Fig. 15. Results of daily-scale dispatch in the islanded mode. (a) Conventional power smoothing control. (b) Proposed control strategy.

1) Grid-Connected Dispatch: In Fig. 14, the microgrid is in the grid-connected mode. P_{POI}^* is changed from 0.2 p.u. (import) to 0 at $t = 1000$ s. For comparative study, conventional power smoothing control with ESS firming short-term renewable and load fluctuation is firstly presented in Fig. 14(a) where SoC of ESS is initially 0.8. With this strategy, diesel generator will be the main contributor to power balance. However, the SoC of ESS stays constant at 0.8 and P_{POI} deviates significantly from its reference at around 1600 s. The result of reactive power dispatch is not shown in the grid-connected mode for brevity.

With the proposed dispatch, the microgrid will have SoC control capability, as demonstrated in Fig. 14(b). For initial SoC at 0.8, dispatch will start from force-discharging control. Diesel generator will output $P_{ds,\min}$ (0.3 p.u.). ESS will thus discharge and SoC drops to SoC_u at $t = 120$ s. After that, power smoothing control will be adopted and SoC is almost constant. However, during heavy-loading intervals when diesel generation is insufficient, ESS will discharge till SoC reaches SoC_{d1} at $t = 1710$ s. Thereafter, ESS will be charged back by slightly increasing the power import P_{POI}, since diesel generator has reached $P_{ds,\max}$. After $t = 1800$ s, power balance and ESS charging will be met by

diesel power solely. In contrast to Fig. 14(a), the impact on the grid in heavy loading intervals is much smaller and SoC of ESS is well addressed for continuous operation. There is no consistent switching between the dispatch modes, which demonstrated the effectiveness of the mode-latching mechanism in Fig. 2. This is also illustrated in Fig. 14(c) where the initial SoC is 0.3.

2) Islanded Dispatch: In Fig. 15, we obtain the results in the islanded mode under the same load/generation condition as in the grid-connected mode. With conventional power-smoothing control, the SoC of ESS will remain almost unchanged, as shown in Fig. 15(a). Load will be shed at around 1600 s. With the proposed dispatch strategy in Fig. 15(b), ESS will discharge during this period thus reducing the load shedding amount. Most of the time, the SoC of ESS will stay around the middle SoC range, which also holds for other initial SoC values.

For reactive power dispatch, the reactive power load, with the power factor of load set around 0.9, is shared among DERs in proportional to their remaining power capacity defined by (7). Since ESS serves as *Vf* reference, the reactive power losses in feeders will also be compensated by ESS, which makes its output power a little larger than the reference calculated from proportional power sharing.

V. Conclusion

This article presents the design and implementation of a centralized MGCS as per the recommended microgrid topology, dispatch methodology, and objectives in IEEE Std 2030.7 and 2030.8. By comprehensive C-HIL testing, we draw the following key conclusions.

1) With rule-based dispatch allowing ESS power smoothing control, ESS force-charging/discharging control, the SoC of ESS can be effectively maintained around 0.5, thus ensuring bidirectional energy reserve. The capability of ESS in peak shaving is also utilized by leaving some SoC margins for ESS to charge or discharge when power mismatch cannot be met by diesel generator.

2) The supplementary slack bus power control is effective in mitigating the fluctuation of power through POI and in compensating for the power mismatch resulting from an open-loop dispatch scheme.

3) Smooth transitions during planned islanding, reconnection and unplanned islanding, are successfully achieved by state-saving techniques, active synchronization, and emergency dispatch, with ESS as the main facilitator.

References

[1] G. Joos, J. Reilly, W. Bower, and R. Neal, "The need for standardization: The benefits to the core functions of the microgrid control system," *IEEE Power Energy Mag.*, vol. 15, no. 4, pp. 32–40, Jul./Aug. 2017.

[2] *IEEE Standard for the Specification of Microgrid Control Systems*, IEEE Std 2030.7-2017, Apr. 23, 2018.

[3] *IEEE Standard for the Testing of Microgrid Controllers*, IEEE Std 2030.8-2018, Aug. 24, 2018.

[4] A. Yamane and S. Abourida, "Real-time simulation of distributed energy systems and microgrids," in *Proc. Int. Conf. Sustain. Mobility Appl., Renewables Technol.*, Kuwait City, Kuwait, 2015, pp. 1–6.

[5] J. H. Jeon *et al.*, "Development of hardware in-the-loop simulation system for testing operation and control functions of microgrid," *IEEE Trans. Power Electron.*, vol. 25, no. 12, pp. 2919–2929, Dec. 2010.

[6] J. Wang, Y. Song, W. Li, J. Guo, and A. Monti, "Development of a universal platform for hardware in-the-loop testing of microgrids," *IEEE Trans. Ind. Informat.*, vol. 10, no. 4, pp. 2154–2165, Nov. 2014.

[7] C. M. Rangel, D. Mascarella, and G. Joos, "Real-time implementation and evaluation of grid-connected microgrid energy management systems," in *Proc. IEEE Elect. Power Energy Conf.*, 2016, pp. 1–6.

[8] Bailu Xiao *et al.*, "Development of hardware-in-the-loop micro-grid testbed," in *Proc. IEEE Energy Convers. Congr. Expo.*, 2015, pp. 1196–1202.

[9] S. Manson *et al.*, "Robust microgrid control system for seamless transition between grid-tied and island operating modes," in *Proc. 44th Annu. Western Protective Relay Conf.*, Oct. 2017.

[10] A. M. Ameen, J. Pasupuleti, and T. Khatib, "Simplified performance models of photovoltaic/diesel generator/battery system considering typical control strategies," *Energy Convers. Manage.*, vol. 99, pp. 313–325, 2015.

[11] C. Sun, J. N. Paquin, F. Al Jajeh, G. Joos, and F. Bouffard, "Implementation and CHIL testing of a microgrid control system," in *Proc. IEEE Energy Convers. Congr. Expo.*, 2018, pp. 2073–2080.

[12] B. Zhao, X. Zhang, P. Li, K. Wang, M. Xue, and C. Wang, "Optimal sizing, operating strategy and operational experience of a stand-alone microgrid on Dongfushan Island," *Appl. Energy*, vol. 113, pp. 1656–1666, 2014.

[13] C. Sun, G. Joos, and F. Bouffard, "Adaptive coordination for power and SoC limiting control of energy storage in islanded AC microgrid with impact load," *IEEE Trans. Power Del.*, to be published, doi: 10.1109/TP-WRD.2019.2916034.

[14] A. Paquette, R. Harley, V. Bhavaraju, S. Krstic, and P. Theisen, "Design of the fort sill microgrid," in *Proc. IEEE Energy Convers. Congr. Expo.*, Pittsburgh, PA, USA, 2014, pp. 4640–4646.

[15] H. Farhangi and G. Joos, *Microgrid Planning and Design: A Concise Guide*. New York, NY, USA: Wiley-IEEE, 2019.

[16] A. Kahrobaeian and Y. A. I. Mohamed, "Analysis and mitigation of low-frequency instabilities in autonomous medium-voltage converter-based microgrids with dynamic loads," *IEEE Trans. Ind. Electron.*, vol. 61, no. 4, pp. 1643–1658, Apr. 2014.

[17] A. Haddadi, A. Yazdani, G. Joos, and B. Boulet, "A generic load model for simulation studies of microgrids," in *Proc. IEEE Power Energy Soc. Gen. Meeting*, Vancouver, BC, Canada, 2013, pp. 1–5.

[18] K. T. Tan, P. L. So, Y. C. Chu, and M. Z. Q. Chen, "Coordinated control and energy management of distributed generation inverters in a microgrid," *IEEE Trans. Power Del.*, vol. 28, no. 2, pp. 704–713, Apr. 2013.

[19] R. E. Moore, R. B. Kearfott, and M. J. Cloud, *Introduction to Interval Analysis*, Cambridge, U.K.: Cambridge Univ. Press, 2009.

[20] S. Bose, Y. Liu, K. Bahei-Eldin, J. de Bedout, and M. Adamiak, "Tieline controls in microgrid applications," in *Proc. Bulk Power System Dyn. Control—VII. Revitalizing Oper. Rel.*, 2007, pp. 1–9.

[21] *IEEE Guide for Design, Operation, and Integration of Distributed Resource Island Systems With Electric Power Systems*, IEEE Std 1547.4-2011, Jul. 20, 2011.

[22] I. J. Balaguer, Q. Lei, S. Yang, U. Supatti, and F. Z. Peng, "Control for grid-connected and intentional islanding operations of distributed power generation," *IEEE Trans. Ind. Electron.*, vol. 58, no. 1, pp. 147–157, Jan. 2011.

[23] X. Chen, Y. H. Wang, and Y. C. Wang, "A novel seamless transferring control method for microgrid based on master-slave configuration," in *Proc. IEEE ECCE Asia Downunder*, Melbourne, VIC, Australia, 2013, pp. 351–357.

[24] T. Zhang, D. Yue, M. J. O'Grady, and G. M. P. O'Hare, "Transient oscillations analysis and modified control strategy for seamless mode transfer in micro-grids: A wind-PV-ES hybrid system case study," *Energies*, vol. 8, pp. 13758–13777, 2015.

[25] Z. Peng *et al.*, "Improved virtual synchronous generator control strategy for seamless switching," in *Proc. IEEE Appl. Power Electron. Conf. Expo.*, San Antonio, TX, USA, 2018, pp. 1003–1007.

[26] J. Wang, N. C. P. Chang, X. Feng, and A. Monti, "Design of a generalized control algorithm for parallel inverters for smooth microgrid transition operation," *IEEE Trans. Ind. Electron.*, vol. 62, no. 8, pp. 4900–4914, Aug. 2015.

[27] Q. Fu, A. Nasiri, V. Bhavaraju, A. Solanki, T. Abdallah, and D. C. Yu, "Transition management of microgrids with high penetration of renewable energy," *IEEE Trans. Smart Grid*, vol. 5, no. 2, pp. 539–549, Mar. 2014.